Protonated 2‘-Aminoguanosine as a Probe of the Electrostatic Environment of the Active Site of the Tetrahymena Group I Ribozyme †

ARTICLE *in* BIOCHEMISTRY · AUGUST 1999

Impact Factor: 3.02 · DOI: 10.1021/bi9903897 · Source: PubMed

3 AUTHORS, INCLUDING:

Songhua Shan
Australian Animal Health Laboratory
21 PUBLICATIONS **935** CITATIONS

SEE PROFILE

Daniel Herschlag
Stanford University
287 PUBLICATIONS **16,539** CITATIONS

SEE PROFILE

Protonated 2′-Aminoguanosine as a Probe of the Electrostatic Environment of the Active Site of the *Tetrahymena* Group I Ribozyme†

Shu-ou Shan,‡ Geeta J. Narlikar,§,|| and Daniel Herschlag*,‡,§

Departments of Biochemistry and Chemistry, Stanford University, Stanford, California 94305

Received February 17, 1999; Revised Manuscript Received May 14, 1999

ABSTRACT: We have probed the electrostatic environment of the active site of the *Tetrahymena* group I ribozyme (E) using protonated 2′-aminoguanosine ($G_{NH_3^+}$), in which the 2′-OH of the guanosine nucleophile (G) is replaced by an -NH_3^+ group. At low concentrations of divalent metal ion (2 mM Mg^{2+}), $G_{NH_3^+}$ binds at least 200-fold stronger than G or G_{NH_2}, with a dissociation constant of ≤ 1 μM from the ribozyme·oligonucleotide substrate·$G_{NH_3^+}$ complex (E·S·$G_{NH_3^+}$). This strong binding suggests that the -NH_3^+ group interacts with negatively charged phosphoryl groups within the active site. Increasing the concentration of divalent metal ion weakens the binding of $G_{NH_3^+}$ to E·S more than 10^2-fold. The Mn^{2+} concentration dependence suggests that M_C, the metal ion that interacts with the 2′-moiety of G in the normal reaction, is responsible for this effect. M_C and $G_{NH_3^+}$ compete for binding to the active site; this competition could arise from electrostatic repulsion between the positively charged -NH_3^+ and M_C and, possibly, from their competition for interaction with active site phosphoryl groups. The reactive phosphoryl group of S increases the competition between M_C and $G_{NH_3^+}$, consistent with a network of interactions involving M_C that help position the reactive phosphoryl group and the guanosine nucleophile with respect to one another. The chemical step with bound $G_{NH_3^+}$ is at least 10^4-fold slower than with G or G_{NH_2}. These results provide additional support for an integral role of M_C in catalysis by the *Tetrahymena* ribozyme, and demonstrate the utility of the -NH_3^+ moiety as an electrostatic probe within a structured RNA.

An RNA enzyme can utilize a variety of functional groups that differ in charge and polarity for building its active site and interacting with its substrates. The backbone of RNA is composed of negatively charged phosphoryl groups; this results in repulsive interactions, but also creates numerous potential binding sites for metal ions and other positively charged groups (e.g., *2*−*15* and references cited therein). The 2′-hydroxyl groups and functional groups on the bases of RNA also provide hydrogen bond donors and acceptors that can interact with each other, with metal ions, and with polar groups on bound ligands (e.g., *3, 4, 6, 8, 9, 11*−*14, 16*−*21,* and references cited therein). The ring moieties of the bases are nonpolar, creating the potential for hydrophobic interactions with each other and with bound ligands (e.g., *19, 21,* and references cited therein).

The energetic effects of electrostatic interactions between functional groups within an RNA also depend on the ability of the RNA to position these groups and to limit active site rearrangements. The *Tetrahymena* group I ribozyme makes extensive interactions with its substrates, which has been suggested to allow precise positioning of substrates and catalytic groups within this RNA active site (*22*−*25* and references cited therein). The interactions within the ribozyme core presumably form an interconnected network to achieve precise positioning. Such a network could also limit rearrangements within the active site, increasing the consequences of electrostatic interactions (e.g., *26*−*29* and references cited therein).

In this work, we have substituted a protonated amine for the 2′-hydroxyl of the guanosine substrate ($G_{NH_3^+}$) to probe the electrostatic environment within the active site of the *Tetrahymena* ribozyme (E).[1] This ribozyme catalyzes the transesterification reaction shown in eq 1, in which an exogenous guanosine nucleophile (G) cleaves a specific phosphodiester bond of the oligonucleotide substrate (S) to generate a shorter oligonucleotide product (P; *30*−*32*).

† This work was supported by NIH Grant GM49243 to D.H.

* Correspondence should be addressed to this author at the Department of Biochemistry, B400 Beckman Center, Stanford University, Stanford, CA 94305-5307. Phone: 650-723-9442. Fax: 650-723-6783. E-mail: herschla@cmgm.stanford.edu.

‡ Department of Biochemistry.

§ Department of Chemistry.

|| Present address: Department of Molecular Biology, Harvard University, Massachusetts General Hospital, Boston, MA 02114.

[1] Abbreviations: E is the L-21 *Sca*I ribozyme; S refers to the oligonucleotide substrate with the sequence $CCCUCUA_5$, without specification of the sugar identity; P refers to the oligonucleotide product, CCCUCU, without specification of the sugar identity. The individual oligonucleotides used in this study are defined in Chart 1. P1 is the duplex formed between the oligonucleotide substrate or product and the internal guide sequence (IGS) of the ribozyme, which has the sequence GGAGGG. $(E·S)_o$ and $(E·S)_c$ refer to the open and closed ribozyme·substrate complexes, respectively, as defined in Figure 7. G is guanosine; G_N refers to 2′-aminoguanosine, without specification of the protonation state of the amino group; $G_{NH_3^+}$ and G_{NH_2} are protonated and deprotonated 2′-aminoguanosine, respectively; and G_X refers to G or G_N. M refers to Mg^{2+} or Mn^{2+}, and M_C refers to the Mg^{2+} or Mn^{2+} ion bound at metal site C.

10.1021/bi9903897 CCC: $18.00
Published on Web 08/06/1999

$$\underset{(S)}{CCCUCU_pA_5} + G_{OH} \rightarrow \underset{(P)}{CCCUCU_{OH}} + G_pA_5 \quad (1)$$

Replacement of the 2′-OH of G with 2′-H decreases the rate of the chemical step more than 10^6-fold (*33*, *34*, and unpublished results). A metal ion interaction with this 2′-OH group has been identified and characterized [Figure 1, M_C (*1*, *35*)]. M_C may facilitate the reaction by helping to deprotonate and activate the 3′-OH of G for nucleophilic attack and by aligning the guanosine nucleophile within the active site (*1*).

Results with the positively charged $G_{NH_3^+}$ suggest the presence of both negatively charged phosphoryl groups and a metal ion near the 2′-moiety of G, and provide additional evidence for a network of active site interactions that involves M_C, the 2′-moiety of G, and the reactive phosphoryl group. The results herein were also necessary to establish conditions that allow investigation of the metal ion interaction with deprotonated 2′-aminoguanosine (G_{NH_2}) in the preceding paper (*1*).

MATERIALS AND METHODS

Materials. Ribozyme was prepared by in vitro transcription with T7 RNA polymerase as described previously (*36*). Oligonucleotides were made by solid phase synthesis and were supplied by the Protein and Nucleic Acid Facility at Stanford University or were gifts from Dr. L. Beigelman (Ribozyme Pharmaceuticals Inc.). Oligonucleotide substrates were 5′-end-labeled using [γ-^{32}P]ATP and T4 polynucleotide kinase and purified by electrophoresis on 24% nondenaturing polyacrylamide gels, as described previously (*37*). 2′-Aminoguanosine was a gift from Dr. F. Eckstein.

General Kinetic Methods. All reactions were single-turnover, with ribozyme in excess of labeled oligonucleotide substrate (S*), and were carried out at 30 °C in 50 mM buffer. The buffers used were the following: sodium acetate, pH 4.4−5.6; NaMES, pH 5.4−7.0; NaMOPS, pH 6.4−7.1; NaHEPES, 6.8−7.5; NaEPPS, pH 7.5−8.5; NaCHES, pH 8.3−9.0. Ribozymes were preincubated in 10 mM $MgCl_2$ and 50 mM buffer at 50 °C for 30 min (*30*, *38*), cooled to 30 °C, and adjusted to the desired metal ion concentrations prior to initiation of the reaction by addition of S* (<0.1 nM). For reactions carried out above pH 8.0, the preincubation was carried out at pH 7.5 to avoid degradation and diluted 10-fold into the appropriate buffer at 30 °C (*39*). Reactions were followed and analyzed as described previously (*30*, *31*, *38*; see also 1).

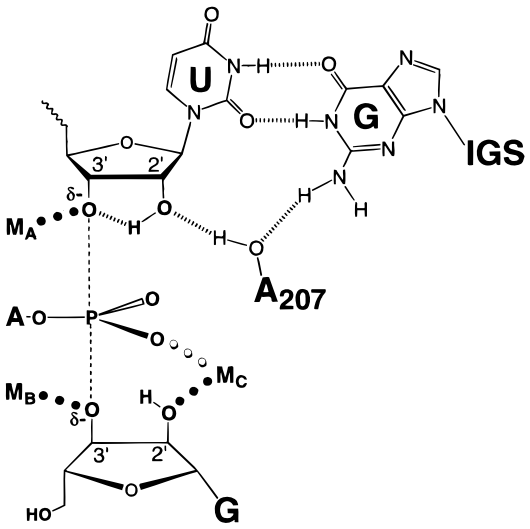

FIGURE 1: Model of transition state interactions within the *Tetrahymena* ribozyme active site. The dashed lines (- - -) depict the partial bond from the reactive phosphorus to the 3′-OH of G and the 3′-oxygen of the U(−1) residue of S. The 2′-OH of U(−1) helps stabilize the neighboring incipient 3′-oxyanion in the transition state (*37* and Yoshida et al., in preparation), and the 2′-hydroxyl group of A207, which bridges the exocyclic amino group of G and the 2′-OH of U, may help orient this 2′-OH (*53*, *58*−*60*). There are three distinct metal ions at the ribozyme active site (Shan et al., submitted). M_A interacts with the 3′-anion of S (*61*). M_B interacts with the 3′-moiety of G (*62*). A third metal ion, M_C, interacts with the 2′-moiety of G (*1*, *35*).

Chart 1[a]

Abbreviation	Oligonucleotide										
		-5		-3		-1	+1	+2		+4	
rSA_5	rC	rC	rC	rU	rC	rU	rA	rA	rA	rA	rA
-1d,rSA_5	rC	rC	rC	rU	rC	dT	rA	rA	rA	rA	rA
-3m,rSA_5	rC	rC	rC	mU	rC	rU	rA	rA	rA	rA	rA
rP	rC	rC	rC	rU	rC	rU					

[a] r = 2′-OH; d = 2′-H; m = 2′-OCH_3.

Reactions were followed for $\geq 3t_{1/2}$ except for very slow reactions. Good first-order fits to the data, with end points of ≥90%, were obtained (KaleidaGraph, Synergy Software, Reading, PA). The slow reactions were typically linear for up to 20 h, and end points of 95% were assumed to obtain observed rate constants from the initial rates.

Determination of the Rate Constant for the Chemical Step: $E{\cdot}S{\cdot}G_X \rightarrow$ Products ($k_c^{G_X}$). Rate constants for reaction from the $E{\cdot}S{\cdot}G_X$ complex (G_X = G or G_N) were determined with the oligonucleotide substrate rSA_5 or -1d,rSA_5 (Chart 1). Values of $k_c^{G_X}$ were determined with ribozyme saturating with respect S ([E] = 50−200 nM; $K_d^S \leq 0.1$ nM) and with saturating G_X (2 mM; $K_d^{G_X} \leq 500$ μM under the conditions investigated; Figures 2, 4, and 5 below). To ensure that the chemical step was rate-determining, the oligonucleotide substrate -1d,rSA_5 was used at pH 5.2−8.5 (*38*, *40*). There is a change in the rate-limiting step for the reaction of rSA_5 above pH 6 (*40* and unpublished results). Replacing the 2′-OH of U(−1) (Chart 1) with 2′-H slows the chemical step ~10^3-fold but has no effect on other reaction steps (*37*, *41*). Below pH 5.2, however, the reaction rate of -1d,rSA_5 is too slow to be accurately determined. To span a wider pH range, the all-RNA substrate rSA_5 was used from pH 4.4 to 5.6. At intermediate pH, reaction rates were determined with both substrates in side-by-side experiments (see Figure 3 below). These experiments showed that the chemical step for rSA_5 is ~700-fold faster than that for -1d,rSA_5. The observed rate constant with -1d,rSA_5 was therefore multiplied by 700 to allow use of the data from both substrates in the pH−rate profile of Figure 3. The following strongly suggest that the chemical step is rate-determining for both substrates over the investigated pH range: (i) the reaction rate has a log-linear dependence on pH; (ii) thio substitution of the *pro-*R_P oxygen of the reactive phosphoryl group slows the observed rate of reaction 2−4-fold (data not shown), consistent with the effects observed in model studies of reactions of phosphate diesters and with previous investigations of the *Tetrahymena* ribozyme (*40*, *42*).

Determination of the Equilibrium Dissociation Constants of G and G_N. Equilibrium constants for binding of G to the $(E\cdot S)_c$ complex (see Figure 7 below) were determined with rSA_5 or -1d,rSA_5 with ribozyme saturating with respect to S ([E] = 50−200 nM; $K_d^S \leq 0.5$ nM). As described in the preceding section, the all-RNA substrate rSA_5 was used below pH 5.6, and -1d,rSA_5 was used from pH 5.2 to 8.5. Within the range of pH used for each oligonucleotide substrate, the chemical step is rate-determining with both saturating and subsaturating G, as described previously (*38, 40*) and in the preceding section. Thus, the dissociation constant of G from E·S·G, K_d^G (Scheme 2), is equal to $K_{1/2}^G$, the concentration of G that provides half the maximal rate (k_{max}) in the dependence of the observed rate of reaction (k_{obsd}) on G concentration (eq 2; see *38* for detailed discussions).

$$k_{obsd} = k_{max} \times \frac{[G_X]}{[G_X] + K_{1/2}^{G_X}} \quad (2)$$

Equilibrium constants for binding of 2′-aminoguanosine (G_N) to the $(E\cdot S)_c$ complex at pH 5.6−8.5 were determined analogously from the G_N concentration dependence of the observed rate of reaction with -1d,rSA_5 (eq 2). Below pH 5.6, however, the rate of the reaction with subsaturating G_N is too slow to be accurately measured. G_N was therefore used instead as a competitive inhibitor of the reaction of G (eq 3a). Under these conditions, G_N binds to E·S* to form a ternary complex that reacts with a negligible rate (Figure 3 under Results), but prevents the binding and reaction of G. With subsaturating G (5−10 μM), the inhibition constant is equal to the dissociation constant of G_N from E·S·G_N ($K_i = K_d^{G_N}$). Values of K_i were determined from the dependence of the observed rate constant (k_{obsd}) on G_N concentration using eq 3b, derived from the reaction scheme in eq 3a. At intermediate pH, both methods were used, and the values of $K_d^{G_N}$ obtained were the same, within experimental error.

$$E\cdot S^* + G \xrightarrow{k_o} \text{products} \quad (3a)$$

$$E\cdot S^*\cdot G_N + G \quad (K_i \pm G_N)$$

$$k_{obsd} = k_o \times \frac{K_i}{K_i + [G_N]} \quad (3b)$$

Equilibrium constants for binding of G_N to the $(E\cdot S)_o$ complex at low pH (5.0) were determined with the oligonucleotide substrate -3m,rSA_5 (Chart 1), which binds E to form a stable open complex (see Figure 7 below). Inhibition methods analogous to those described above were used (eq 3a,b).

Equilibrium constants for binding of G_X to the ribozyme·oligonucleotide product complex (E·P) were determined using G or G_N as a competitive inhibitor of the reverse reaction (eq 4a), as G_X can bind to E·P and prevent binding and reaction of 5′-labeled GA (*GA). The inhibition constant, K_i, is equal to the dissociation constant of G_X from E·P·G_X under conditions such that E·P is subsaturating with respect to trace amounts of *GA [<0.1 nM *GA; 0.2−1 μM E·P; $K_d^{GA} \approx 300$ μM (*43* and R. Russell and D.H., unpublished results)]. The value of K_i was obtained from the dependence of the observed rate constant of the reverse reaction (k_{obsd}) on G_X concentration using eq 4b, derived from eq 4a.

$$E\cdot P + {}^*GA \xrightarrow{k_o} E\cdot S + {}^*G_{OH} \quad (4a)$$

$$E\cdot P\cdot G_X + {}^*GA \quad (K_i \pm G_X)$$

$$k_{obsd} = k_o \times \frac{K_i}{K_i + [G_X]} \quad (4b)$$

Determination of the pK_a of 2′-Aminoguanosine in Solution and in the E·S·G_N Complex. The different reactivities of $G_{NH_3^+}$ and G_{NH_2} in the reaction: E·S·G_X → products provide a signal for deprotonation of the -NH_3^+ group in the E·S·G_N complex (Figure 3 below). Values of $pK_{a,app}^{E\cdot S\cdot G_N}$, the negative logarithm of the observed equilibrium constant for deprotonation of $G_{NH_3^+}$ in E·S·G_N, were obtained from the pH dependence of the rate of the chemical step with G_N relative to G, $k_{c,rel}$. The data were fit to eq 5, which was derived from Scheme 1 under Results. $k_{c,rel}^{obsd}$ is the observed rate of reaction of G_N relative to G at each pH, and $k_{c,rel}^{G_{NH_3^+}}$ and $k_{c,rel}^{G_{NH_2}}$ are the pH-independent rate constants for reaction of G_N in the protonated and deprotonated state, respectively, relative to G. As described under Results, these are apparent pK_a values because protonation of the 2′-amino group is coupled to dissociation of a metal ion from site C.

$$k_{c,rel}^{obsd} = k_{c,rel}^{G_{NH_2}} \times \frac{K_{a,app}^{E\cdot S\cdot G_N}}{K_{a,app}^{E\cdot S\cdot G_N} + [H^+]} + k_{c,rel}^{G_{NH_3^+}} \times \frac{[H^+]}{K_{a,app}^{E\cdot S\cdot G_N} + [H^+]} \quad (5)$$

The pH dependence of the observed binding constant of G_N for E·S, $K_b^{G_N}$, allowed determination of the equilibrium constant for deprotonation of the -NH_3^+ group of free G_N, $K_a^{G_N}$ (*44*). As varying the pH does not significantly alter the binding of G, it was unnecessary to correct the effects of pH common to G and G_N (see Figure 4 and Results). The data were fit to eq 6, which was derived from Scheme 3 under Results; $K_{b,obsd}^{G_N}$ is the observed binding constant of G_N at a particular pH, and $K_b^{G_{NH_2}}$ and $K_b^{G_{NH_3^+}}$ are the binding constants of G_{NH_2} and $G_{NH_3^+}$, respectively.

$$K_{b,obsd}^{G_N} = K_b^{G_{NH_2}} \times \frac{K_a^{G_N}}{K_a^{G_N} + [H^+]} + K_b^{G_{NH_3^+}} \times \frac{[H^+]}{K_a^{G_N} + [H^+]} \quad (6)$$

Determination of the Dissociation Constants of Mg^{2+} and Mn^{2+}. Mg^{2+} and Mn^{2+} (M^{2+}) weaken the binding of G_N to E·S at low pH, providing a signal for binding of these metal ions to the E·S and E·S·G_N complexes. The affinity of G_N follows metal ion concentration dependences for an effect from a single Mg^{2+} or Mn^{2+} (Figure 4B,C below). The following suggest that the metal ions studied herein achieve equilibrium binding prior to the chemical step so that the

concentration of Mg^{2+} or Mn^{2+} required to obtain half of the observed change, $K^{M}_{1/2}$, equals the dissociation constant of the metal ion from the ribozyme·substrate complexes (see also ref *1*): (i) the reaction rate is not affected by the time of preincubation with metal ions prior to initiation of the reaction, nor by the order of addition or dilution of metal ions and other reaction components; (ii) reactions follow good first-order kinetics without observation of any burst or lag phase; (iii) the $K^{M}_{1/2}$ value for E·S is the same at pH 4.4 and 5.0, despite the ~10-fold difference in reaction rate.

The apparent dissociation constant of Mn^{2+} from the E·S binary complex, $K^{Mn,app}_{E\cdot S}$, was obtained from the Mn^{2+} concentration dependence of the equilibrium binding constant of G_N at low pH.[2] The data were fit to eq 7, which was derived from Scheme 5 under Results; $K^{G_N}_{b,obsd}$ is the observed binding constant of G_N at a particular Mn^{2+} concentration, and $K^{G_{NH_3^+}}_{b,app}$ and $K^{G_N}_{b,Mn}$ are the binding constants of G_N with zero and saturating Mn^{2+}, respectively.

$$K^{G_N}_{b,obsd} = K^{G_N}_{b,Mn} \times \frac{[Mn^{2+}]}{[Mn^{2+}] + K^{Mn,app}_{E\cdot S}} + K^{G_{NH_3^+}}_{b,app} \times \frac{K^{Mn,app}_{E\cdot S}}{[Mn^{2+}] + K^{Mn,app}_{E\cdot S}} \quad (7)$$

The dependence of the dissociation constant of G_N ($K^{G_N}_{d}$) on the concentration of Mg^{2+} or Mn^{2+} at low pH allowed determination of the dissociation constant of Mg^{2+} or Mn^{2+} from the E·S·G_N ternary complex, $K^{M}_{E\cdot S\cdot G_N}$.[2] The data were fit to eq 8, also derived from Scheme 5, in which $K^{G_N}_{d,obsd}$ is the observed dissociation constant of G_N at a particular concentration of the metal ion being varied (Mg^{2+} or Mn^{2+}), $K^{G_N}_{d}$ is the dissociation constant of G_N with the metal site unoccupied, and $K^{G_N}_{d,M}$ is the observed dissociation constant of G_N with the varied metal ion saturating.

$$K^{G_N}_{d,obsd} = K^{G_N}_{d,M} \times \frac{[M^{2+}]}{[M^{2+}] + K^{M}_{E\cdot S\cdot G_N}} + K^{G_N}_{d} \times \frac{K^{M}_{E\cdot S\cdot G_N}}{[M^{2+}] + K^{M}_{E\cdot S\cdot G_N}} \quad (8)$$

RESULTS

We first present evidence that $G_{NH_3^+}$ is catalytically inactive. The next section describes results that suggest that $G_{NH_3^+}$ binds stronger than G and G_{NH_2}. The ability of Mg^{2+} and Mn^{2+} to weaken the binding of $G_{NH_3^+}$ to the E·S complex is then described, along with evidence that the metal ion at site C is responsible (Figure 1, M_C). The thermodynamic framework of Figure 2 summarizes the effect of M_C on the binding of $G_{NH_3^+}$ to E·S described in this section and its effect on the binding of neutral G_{NH_2} (*1*). This framework also summarizes the equilibrium constants for deprotonation of the -NH_3^+ group in solution and in the E·S·G_N complex; these constants were necessary to determine reaction conditions for investigation of the binding and reactivity of $G_{NH_3^+}$ herein and of G_{NH_2} in the preceding paper. The last section of the Results explores the effect of the oligonucleotide substrate on the repulsive interactions between $G_{NH_3^+}$ and M_C.

$G_{NH_3^+}$ Is at Least 10^4-Fold Less Reactive than G in the Chemical Step. The 2′-NH_3^+ group of $G_{NH_3^+}$ has no lone pair electrons and therefore cannot interact with a metal ion. We first asked how this modification affects the reactivity of the guanosine nucleophile. The rate constant of the reaction E·S·G_N → products ($k^{G_N}_{c}$) was measured from pH 4.4 to 8.5 with saturating G_N (Figure 3A, closed symbols). The chemical step for G_N has a steep dependence on pH, with a slope of 2 below pH 7.5, and becomes less steep at higher pH. To isolate the effects of pH that arise from protonation of G_N, the pH dependence of the rate of reaction: E·S·G → products was determined in parallel. The chemical step for G is log-linear with pH with a slope of 1 (Figure 3A, open symbols), consistent with previous observations (*40*).

The rate effect that stems specifically from protonation of G_N was analyzed from the pH dependence of the rate of reaction of G_N relative to G (Figure 3B, $k_{c,rel}$). The reaction of G_N is more than 10^4-fold slower than G at the lowest pH (4.4). As the reaction rate continues to decrease at low pH, the chemical step for $G_{NH_3^+}$ is at least 10^4-fold slower than G (Scheme 1, $k^{G_{NH_3^+}}_{c,rel}$). The relative reactivity of G_N increases log-linearly with pH with a slope of 1 below pH 7.2 (Figure 3B); at higher pH, the relative reactivity of G_N levels off at a rate within 5-fold of the reaction of G, corresponding to reaction of G_{NH_2} (Scheme 1, $k^{G_{NH_2}}_{c,rel} = 0.2$; see also *1*). Fitting the pH dependence of $k_{c,rel}$ to the model in Scheme 1 gives an apparent pK_a value of $pK^{E\cdot S\cdot G_N}_{a,app} = 7.5 \pm 0.3$ for deprotonation of the 2′-NH_3^+ group in the E·S·G_N complex at 10 mM Mg^{2+} (the pK_a is apparent because protonation of the 2′-amino group is coupled to dissociation of a Mg^{2+} ion from the ribozyme, as described below).

$G_{NH_3^+}$ Binds More Strongly to E·S than G and G_{NH_2}. Equilibrium constants for binding of G_N and G (G_X) to the E·S complex (Scheme 2, $K^{G_X}_{b}$) were determined from pH

[2] The binding constant, $K^{G_N}_{b}$, or the dissociation constant, $K^{G_N}_{d}$ (=1/$K^{G_N}_{b}$), is used in plotting and describing the experimental results, depending on whether the E·S or E·S·G_N complex is the focus of discussion. $K^{G_N}_{b}$ monitors the association process: E·S + G_N → E·S·G_N, such that plots of $K^{G_N}_{b}$ versus metal ion concentration directly give the metal ion dissociation constant from the E·S complex. On the other hand, $K^{G_N}_{d}$ monitors the dissociation process: E·S·G_N → E·S + G_N, such that plots of $K^{G_N}_{d}$ versus metal ion concentration directly give the metal ion dissociation constant from the E·S·G_N complex (*44*).

[3] The affinity of G for the E·S complex weakens below pH 5.6, probably due to disruption of ribozyme structure at low pH. Above pH 5.6, binding of G is strengthened by bound S, whereas this coupled binding of G with S is lost at lower pH (*1* and D. S. Knitt and D.H., unpublished results). However, the loss of coupling between G and S at low pH is not expected to affect the pH dependence of G_N binding, because binding of G_{NH_2} is not coupled to S binding [10 mM Mg^{2+} (*1*)]. Thus, the weakening of the affinity of G below pH 5.6 was not corrected in analysis of the pH dependence of G_N binding to obtain the binding constant for $G_{NH_3^+}$ (Scheme 3). Correction of this effect would render the binding constant for $G_{NH_3^+}$ that was obtained a lower limit for the binding of $G_{NH_3^+}$ to the intact ribozyme active site. The following strongly suggest that the analysis without this correction is appropriate: (i) the data fit well to eq 6, which is derived based on this assumption; (ii) the solution pK_a of G_N ($pK^{G_N}_{a}$) obtained from this fit is consistent with the previous determination (*45*); (iii) the pK_a of the E·S·G_N complex ($pK^{E\cdot S\cdot G_N}_{a,app}$) obtained from this analysis is in good agreement with the value determined in independent experiments (see text).

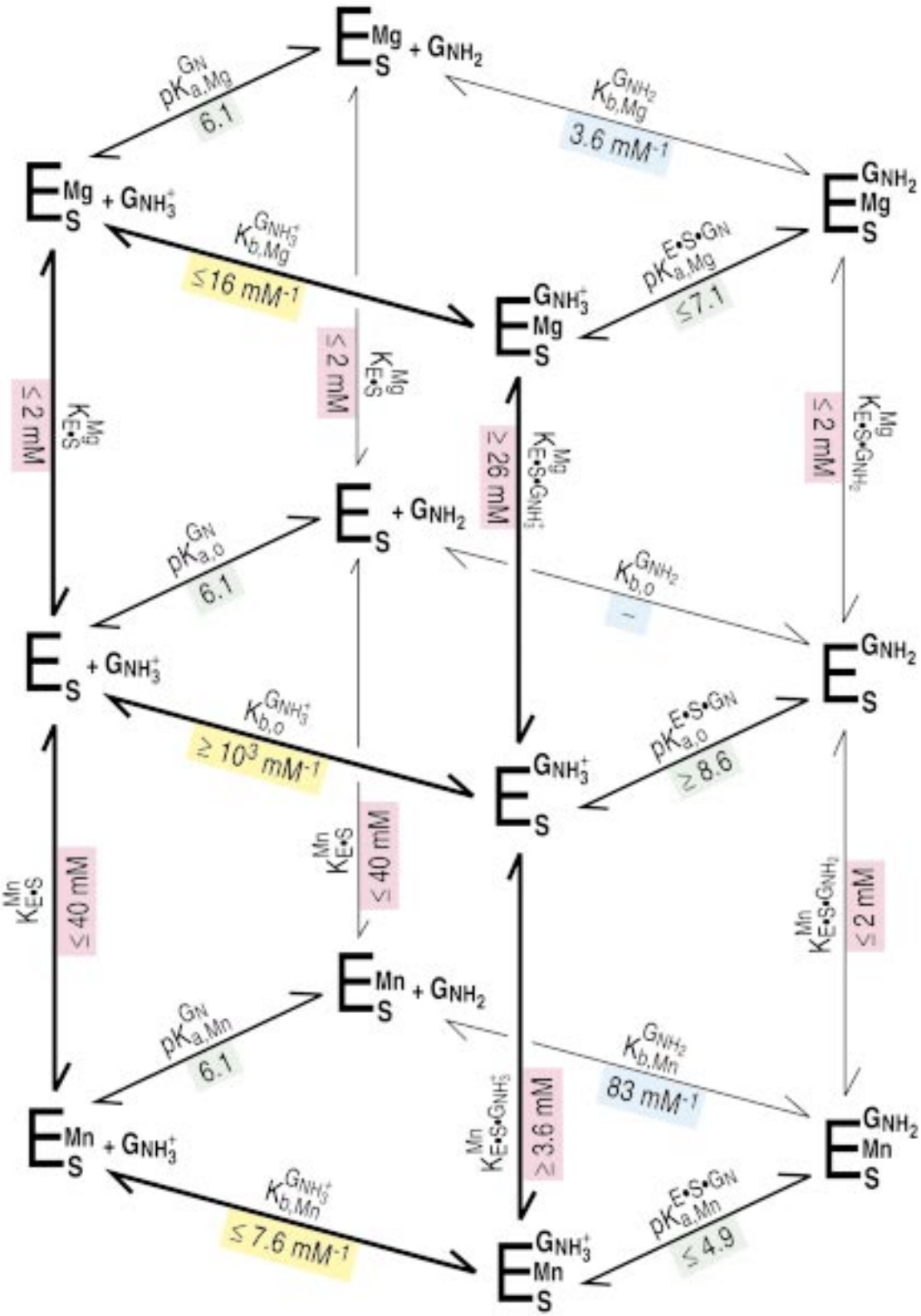

FIGURE 2: Thermodynamic framework summarizing the effect of the Mg^{2+} or Mn^{2+} bound at metal site C (Mg_C^{2+} and Mn_C^{2+}, respectively) on the binding of $G_{NH_3^+}$ (thick arrows in foreground) or G_{NH_2} (thin arrows in background) to the $(E{\cdot}S)_c$ complex. Equilibrium constants for binding of $G_{NH_3^+}$ and for binding of Mg_C^{2+} and Mn_C^{2+} to the $E{\cdot}S{\cdot}G_{NH_3^+}$ complex (numbers in yellow and pink, respectively, in the foreground) were determined with the oligonucleotide substrate rSA_5 (Chart 1) and are described under Results. Determination of the equilibrium constants for deprotonation of the 2′-group in solution and in the $E{\cdot}S{\cdot}G_N$ complexes (numbers in green) is also described under Results. The equilibrium constants for binding of G_{NH_2} and binding of Mg_C^{2+} and Mn_C^{2+} to the E·S and $E{\cdot}S{\cdot}G_{NH_2}$ complexes were determined and described in the preceding paper (*1*). −, not determined.

4.4 to 8.5 under the conditions used in Figure 3; the binding constants are shown in Figure 4.

Below pH 5, G_N binds to the E·S complex 25-fold more strongly than G. Binding of G_N weakens with increasing pH

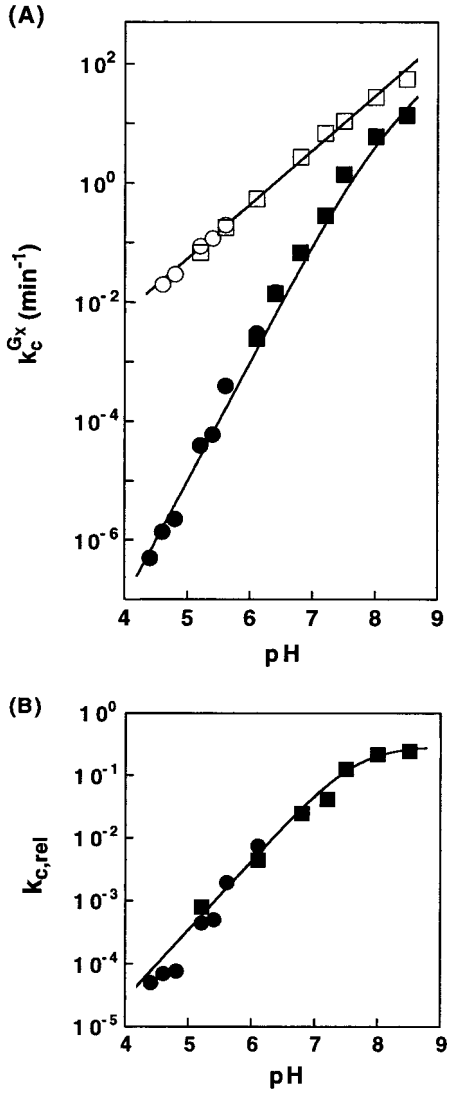

FIGURE 3: $E{\cdot}S{\cdot}G_{NH_3^+}$ is less reactive than $E{\cdot}S{\cdot}G_{NH_2}$ in the chemical step. (A) pH dependence of the rate constant of the reaction: $E{\cdot}S{\cdot}G_X \rightarrow$ products (k_c^{Gx}) for G_N (●, ■) and G (○, □) at 10 mM Mg^{2+}, determined as described under Materials and Methods. Reactions were followed with rSA_5 (●, ○) and -1d,rSA_5 (■, □). To correct for the effect of the 2′-H substitution on the rate of the chemical step and allow direct comparison with the reaction rates of rSA_5, the rate constants for -1d,rSA_5 were multiplied by 700, a factor determined from side-by-side measurements with both substrates at intermediate pH (see Materials and Methods). (B) pH dependence of the reactivity of G_N relative to G, $k_{c,rel} = k_c^{G_N}/k_c^G$, with rSA_5 (●) and -1d,rSA_5 (■). Values of k_c^G and $k_c^{G_N}$ are from part A. The line is a fit of the data to eq 5, derived from Scheme 1 (see Materials and Methods), and gives $pK_{a,app}^{E{\cdot}S{\cdot}G_N} = 7.5$ (10 mM Mg^{2+}).

and levels off above pH 7.5 (closed symbols), whereas the binding of G to E·S does not change significantly from pH 5.6 to 8.5 (open symbols).[3] These data suggest that $G_{NH_3^+}$

[4] The binding constant of $G_{NH_3^+}$ is apparent because $G_{NH_3^+}$ binding is coupled to dissociation of a Mg^{2+} ion from site C (see Figure 2); in contrast, a Mg^{2+} ion is bound at site C in both the E·S and $E{\cdot}S{\cdot}G_{NH_2}$ complexes at 10 mM Mg^{2+} (*1*), and this is denoted by the subscript 'Mg' in the binding constant for G_{NH_2} (Scheme 3, $K_{b,Mg}^{G_{NH_2}}$). Similarly, the pK_a of the $-NH_3^+$ group in $E{\cdot}S{\cdot}G_N$ observed under these conditions is an apparent pK_a value because protonation is coupled to Mg^{2+} dissociation (Scheme 1 and Scheme 3, $pK_{a,app}^{E{\cdot}S{\cdot}G_N}$).

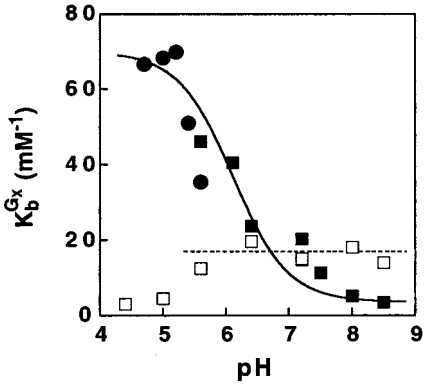

FIGURE 4: pH dependence of the binding of G and G_N to E·S, K_b^{Gx}. Equilibrium binding constants for G_N and G were determined at 10 mM Mg^{2+} from the dependence of the observed rate of reaction on G_N or G concentration (■, □) or from inhibition methods (●) (see Materials and Methods). The solid line is a fit of the data of G_N to eq 6, derived from Scheme 2 (see Materials and Methods), and gives $pK_a^{G_N} = 6.1 \pm 0.2$ for deprotonation of $G_{NH_3^+}$ in solution, and $K_{b,app}^{G_{NH_3^+}} = 67$ and $K_{b,Mg}^{G_{NH_2}} = 3.6$ mM^{-1} for binding of $G_{NH_3^+}$ and G_{NH_2} to E·S, respectively. The dashed line highlights that binding of G is constant above pH 5.6.[3]

Scheme 1

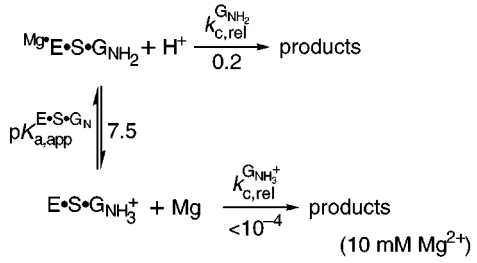

Scheme 2

$$E{\cdot}S + G_X \overset{K_b^{Gx}}{\rightleftharpoons} E{\cdot}S{\cdot}G_X$$

$$K_b^{Gx} = 1/K_d^{Gx} = \frac{[E{\cdot}S{\cdot}G_X]}{[E{\cdot}S][G_X]}$$

Scheme 3

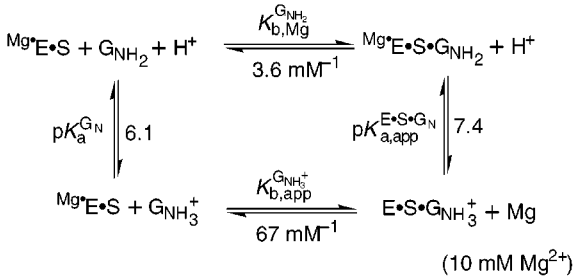

binds more strongly than G or G_{NH_2} to E·S. A fit of the pH dependence of the binding of G_N to the model of Scheme 3 (Figure 4, solid line) gives binding constants of $K_{b,app}^{G_{NH_3^+}} = 67$ mM^{-1} and $K_{b,Mg}^{G_{NH_2}} = 3.6$ mM^{-1}, respectively.[4] This fit also gives a pK_a value of 6.1 ± 0.2 for deprotonation of $G_{NH_3^+}$ in solution (Scheme 3, $pK_a^{G_N}$), the same as the solution pK_a of 6.2 determined directly for the 2′-amino group within a dinucleotide (*45*). This solution pK_a and the 19-fold stronger binding of $G_{NH_3^+}$ than G_{NH_2} predict that $G_{NH_3^+}$ deprotonates

with an apparent pK_a value of $pK_{a,app}^{E\cdot S\cdot G_N} = 7.4$ in the E·S·G_N complex [Scheme 3; $K_{a,app}^{E\cdot S\cdot G_N} = K_a^{G_N} \times (K_{b,Mg}^{G_{NH_2}}/K_{b,app}^{G_{NH_3^+}}) = 10^{-6.1} \times (3.6/67) = 10^{-7.4}$, $pK_{a,app}^{E\cdot S\cdot G_N} = -\log K_{a,app}^{E\cdot S\cdot G_N} = 7.4$]. This is the same, within error, as the value of $pK_{a,app}^{E\cdot S\cdot G_N} = 7.5$ obtained independently (Figure 3).

Mg^{2+} and Mn^{2+} Weaken the Binding of $G_{NH_3^+}$. The stronger binding of $G_{NH_3^+}$ than G and G_{NH_2} described above was surprising, as previous studies showed that metal site C, which is situated near the 2′-moiety of G in the E·S·G and E·S·G_{NH_2} complexes, is occupied by a Mg^{2+} ion at concentrations above 2 mM [Figure 1, M_C (*1*)]. We therefore investigated the effect of metal ions on the binding of $G_{NH_3^+}$ to E·S. The results showed that addition of Mg^{2+} or Mn^{2+} weakens the binding of $G_{NH_3^+}$ to E·S and that this effect can be attributed to M_C, the metal ion that interacts with the 2′-moiety of G in the normal reaction.

The effects of Mg^{2+} or Mn^{2+} at site C (Mg_C^{2+} and Mn_C^{2+}, respectively) on the binding of $G_{NH_3^+}$ and G_{NH_2} to E·S are summarized in the thermodynamic framework of Figure 2, which serves as a guide for describing the determination of individual equilibrium constants in this and the next section. Figure 2 contains three thermodynamic cycles stacked upon one another. The top and bottom planes are thermodynamic cycles with metal site C occupied by a Mg^{2+} or Mn^{2+}, respectively, and the middle plane is a cycle with site C unoccupied. Each cycle depicts the equilibrium for binding of $G_{NH_3^+}$ and G_{NH_2} to E·S ($K_b^{G_{NH_3^+}}$ and $K_b^{G_{NH_2}}$, respectively) and the equilibrium for deprotonation of the 2′-NH_3^+ group in solution and in the E·S·G_N complex ($pK_a^{G_N}$ and $pK_a^{E\cdot S\cdot G_N}$, respectively). The subscript 'Mg' or 'Mn' in these equilibrium constants denotes the metal ion bound at site C, and the subscript 'o' denotes that site C is unoccupied. The vertical arrows that connect the top and middle planes are the equilibrium dissociation constants of Mg_C^{2+} (K^{Mg}), and those that connect the middle and bottom planes, the equilibrium dissociation constants of Mn_C^{2+} (K^{Mn}). The subscripts in these metal ion dissociation constants depict the ribozyme·substrate species that binds Mg_C^{2+} or Mn_C^{2+}; e.g., $K_{E\cdot S}^{Mn}$ is the dissociation constant of Mn_C^{2+} from the E·S complex.

The equilibrium constants for binding of $G_{NH_3^+}$ to E·S and the effects of M_C on $G_{NH_3^+}$ binding (Figure 2, thick arrows) were determined by experiments described in this section. Quantitating the equilibrium constants for deprotonation of the 2′-NH_3^+ group in solution and in the E·S·G_N complexes is crucial for investigation of the binding and reactivity of $G_{NH_3^+}$ and G_{NH_2} in this and the preceding paper (*1*); the determination of these equilibrium constants is described in the next section. To complete the thermodynamic cycles and to allow comparison with the $G_{NH_3^+}$ results, the effects of M_C on the binding of G_{NH_2} to E·S are also shown (thin arrows; *1*).

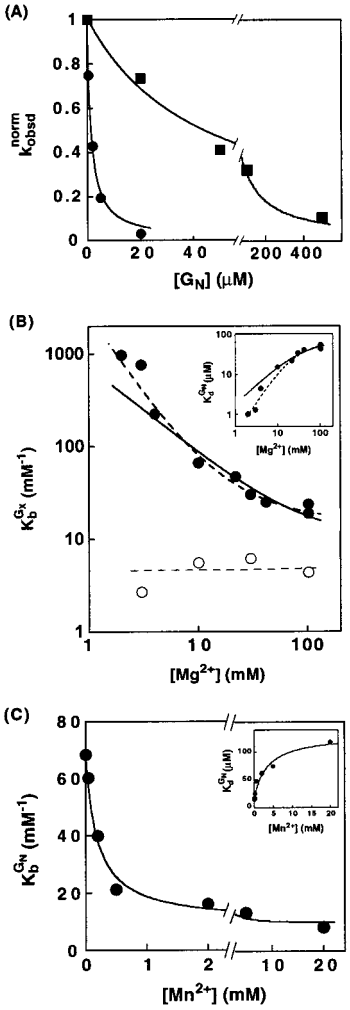

FIGURE 5: Mg^{2+} and Mn^{2+} weaken the binding of $G_{NH_3^+}$ to the $(E\cdot S)_c$ complex (S = rSA_5). (A) Binding of $G_{NH_3^+}$ to E·S at 2 mM (●) and 100 mM Mg^{2+} (■), determined by inhibition of the reaction of G with $G_{NH_3^+}$ at pH 4.7 (see Materials and Methods). (B) Effect of [Mg^{2+}] on the equilibrium binding constant of $G_{NH_3^+}$ (●) and G (○) at pH 4.7 [from part A and analogous experiments].[2] The solid line is a fit of the data of $G_{NH_3^+}$ to the model in Scheme 4, and gives a binding constant for $G_{NH_3^+}$ of 16 mM^{-1} with saturating Mg^{2+}. The dashed curve is a fit of the data to a model in which two Mg^{2+} ions decrease the binding of $G_{NH_3^+}$. The dashed straight line shows that binding of G is not affected by changes in Mg^{2+} concentration. The insert shows the Mg^{2+} concentration dependence of the dissociation constant of G_N from E·S·G_N, $K_d^{G_N}$. The solid line is a fit of the data to eq 8, derived from Scheme 4, and gives an apparent Mg^{2+} dissociation constant of $K_{E\cdot S\cdot G_N}^{Mg} = 26 \pm 4$ mM (see Materials and Methods). The dashed line is a fit of the data to a model involving two Mg^{2+} ions. (C) Effect of [Mn^{2+}] on the binding of G_N to E·S at pH 5.0 with 10 mM Mg^{2+}, determined by experiments analogous to part A. The solid line is a fit of the data to eq 7, derived from Scheme 5, and gives an apparent Mn^{2+} dissociation constant of $K_{E\cdot S}^{Mn,app} = 0.19 \pm 0.03$ mM and a binding constant for G_N of $K_{b,Mn}^{G_N} = 7.6$ mM^{-1} (see Materials and Methods). The insert shows the Mn^{2+} concentration dependence of the dissociation constant of G_N from E·S·G_N, $K_d^{G_N}$. The solid line is a fit of the data to eq 8, derived from Scheme 5, and gives an apparent Mn^{2+} dissociation constant of $K_{E\cdot S\cdot G_N}^{Mn} = 3.6 \pm 0.6$ mM (see Materials and Methods).

[5] The following strongly suggest that the binding of G_N to E·S (S = rSA_5) observed at pH 4.7 reflects the binding of $G_{NH_3^+}$ over the entire range of Mg^{2+} concentration investigated (2−100 mM). G_{NH_2} binds weaker to E·S than $G_{NH_3^+}$ in Mg^{2+}; the binding constant for G_{NH_2} is ∼3 mM^{-1} from 2 to 100 mM Mg^{2+} (*1* and data not shown), whereas the binding constant for G_N at pH 4.7 is ≥20 mM^{-1} over the entire Mg^{2+} concentration range investigated (Figure 5B). Thus, the small fraction of G_{NH_2} present at pH 4.7 (0.04, $pK_a^{G_N} = 6.1$) makes a negligible contribution to the binding of G_N at this pH.

Scheme 4

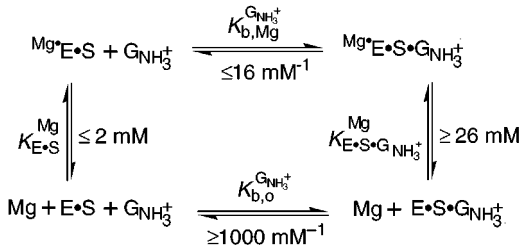

(A) Mg^{2+} Weakens the Binding of $G_{NH_3^+}$ More than 60-Fold. Figure 5A shows that $G_{NH_3^+}$ binds strongly to E·S at low Mg^{2+} concentrations, with a binding constant of 1000 mM^{-1} at 2 mM Mg^{2+}; in contrast, binding of $G_{NH_3^+}$ is 50-fold weaker at 100 mM Mg^{2+}.[5] The binding of $G_{NH_3^+}$ weakens with increasing [Mg^{2+}] and levels off above 40 mM Mg^{2+}, whereas the binding of G is the same, within error, as the Mg^{2+} concentration is increased from 3 to 100 mM (Figure 5B).

The Mg^{2+} concentration dependence of the binding of $G_{NH_3^+}$ above 4 mM Mg^{2+} is consistent with the effect expected for a single Mg^{2+} (Figure 5B, solid line). As the Mg^{2+} concentration decreases from 4 to 2 mM, the affinity of $G_{NH_3^+}$ increases 4-fold, twice the effect predicted for an effect from a single Mg^{2+}. This small deviation could be caused by an effect of Mg^{2+} on ribozyme structure or by electrostatic repulsion from binding of additional Mg^{2+}. Inclusion of a second Mg^{2+} slightly improves the fit of the data below 4 mM Mg^{2+} (Figure 5B, dashed line), but does not significantly change the Mg^{2+} and $G_{NH_3^+}$ binding constants obtained. We therefore use the simpler model in which a single Mg^{2+} ion weakens the binding of $G_{NH_3^+}$ (Scheme 4).[6]

Analysis of the data of Figure 5B according to the model of Scheme 4 allowed estimation of limits for the individual equilibrium constants. The binding of $G_{NH_3^+}$ continues to increase at the lowest Mg^{2+} concentrations; thus, the value of 1000 mM^{-1} observed at 2 mM Mg^{2+} represents a lower limit for the binding of $G_{NH_3^+}$ with the metal site unoccupied (Scheme 4, $K_{b,o}^{G_{NH_3^+}}$). The continued increase of $G_{NH_3^+}$ binding at low [Mg^{2+}] also suggests that the Mg^{2+} responsible for this effect binds to E·S tightly, with a dissociation constant of $K_{E\cdot S}^{Mg} \leq 2$ mM (Scheme 4). The effect of Mg^{2+} on $G_{NH_3^+}$ binding appears to saturate at high Mg^{2+} concentration. This could arise from saturation of a specific Mg^{2+} site that weakens the binding of $G_{NH_3^+}$ or from a distinct Mg^{2+} ion (or ions) that antagonizes the effect of the Mg^{2+} that weakens $G_{NH_3^+}$ binding. Thus, the binding constant for $G_{NH_3^+}$ extrapolated to saturating Mg^{2+}, 16 mM^{-1} (Figure 5B), represents an upper limit for the affinity of $G_{NH_3^+}$ with saturating Mg^{2+}, $K_{b,Mg}^{G_{NH_3^+}}$ (Scheme 4). For the same reason, although the Mg^{2+} concentration dependence of $K_d^{G_{NH_3^+}}$ gives an apparent Mg^{2+} dissociation constant of 26 mM for the ternary complex (Figure 5B insert),[2] this value is a lower limit for the dissociation constant of the Mg^{2+} ion that weakens $G_{NH_3^+}$ binding (Scheme 4, $K_{E\cdot S\cdot G_{NH_3^+}}^{Mg}$).

[6] Scheme 4 is a portion of the thermodynamic framework of Figure 2, presented to simplify the description of the determination of individual equilibrium constants in the text.

Scheme 5

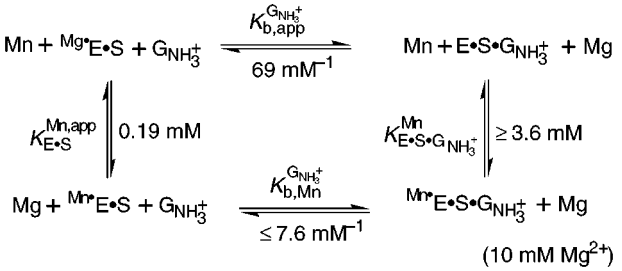

The ability of Mg^{2+} to weaken the binding of $G_{NH_3^+}$ and the affinity of this Mg^{2+} ion for the E·S complex (Scheme 4, $K_{E\cdot S}^{Mg} \leq 2$ mM) are consistent with an effect from Mg_C^{2+}, which is situated near the 2′-moiety of G in the $E\cdot S\cdot G_{NH_3^+}$ complex (Figure 1B; *1*). To test whether M_C is indeed responsible for the weakened binding of $G_{NH_3^+}$, we investigated the effect of added Mn^{2+}.

(B) Mn_C^{2+} Decreases the Binding of $G_{NH_3^+}$ More than 100-Fold. If M_C is responsible for the weakened binding of $G_{NH_3^+}$, then Mn^{2+} should also weaken the binding of $G_{NH_3^+}$, as Mn^{2+} binds strongly to site C (*1*). Further, the Mn^{2+} ion that weakens the binding of $G_{NH_3^+}$ should have the affinity characteristic of Mn_C^{2+} (*1*).

Figure 5C shows that addition of Mn^{2+} does indeed weaken the binding of $G_{NH_3^+}$, whereas addition of Mn^{2+} has no effect on binding of G at corresponding pH values (data not shown). The Mn^{2+} concentration dependence suggests that a single Mn^{2+} ion binds to the E·S complex and weakens the binding of $G_{NH_3^+}$ (Scheme 5). The fit of the data in Figure 5C to the model of Scheme 5 gives an apparent dissociation constant of $K_{E\cdot S}^{Mn,app} = 0.19 \pm 0.03$ mM for binding of the Mn^{2+} ion to E·S.[7] This is the same, within error, as the affinity of Mn_C^{2+} determined previously ($K_{E\cdot S}^{Mn,app} = 0.21$ mM; 10 mM Mg^{2+}; *1*). The agreement between the Mn^{2+} affinities strongly suggests that the metal ion at site C is responsible for weakening the binding of $G_{NH_3^+}$.

The data in Figure 5C also allow estimation of the affinity of $G_{NH_3^+}$ for E·S with Mn^{2+} bound at site C (Scheme 5, $K_{b,Mn}^{G_{NH_3^+}}$) and the affinity of Mn_C^{2+} for the $E\cdot S\cdot G_{NH_3^+}$ complex (Scheme 5, $K_{E\cdot S\cdot G_{NH_3^+}}^{Mn}$). With saturating Mn^{2+}, the binding constant of G_N is 7.6 mM^{-1} (Figure 5C). This value is an upper limit for $K_{b,Mn}^{G_{NH_3^+}}$, the binding constant of $G_{NH_3^+}$ with Mn^{2+} bound at site C. This is because G_{NH_2} binds strongly to E·S with Mn_C^{2+} bound (Figure 2, $K_{b,Mn}^{G_{NH_2}} = 83$ mM^{-1}; *1*); thus, the fraction of G_{NH_2} present at pH 5.0 (0.08, $pK_a^{G_N} = 6.1$) may be responsible for a substantial amount of the observed binding of G_N under these conditions. For the same reason, although the Mn^{2+} concentration dependence of $K_d^{G_N}$ at pH 5.0 (Figure 5C, insert) gives an observed Mn_C^{2+} dissociation constant of 3.6 mM, this value is only a lower limit for $K_{E\cdot S\cdot G_{NH_3^+}}^{Mn}$, the dissociation constant of Mn_C^{2+} from the $E\cdot S\cdot G_{NH_3^+}$ complex (Scheme 5).[8]

[7] $K_{E\cdot S}^{Mn,app}$ is an apparent Mn^{2+} dissociation constant because this Mn^{2+} ion, Mn_C^{2+}, competes with a Mg^{2+} bound at site C in the E·S complex (*1*).

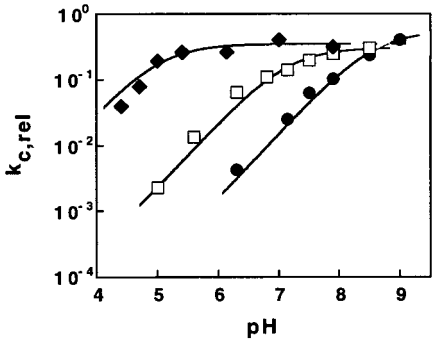

FIGURE 6: Determinations of the pK_a of the -NH_3^+ group in the E·S·G_N complex at 2 mM Mg^{2+} (●), 100 mM Mg^{2+} (□), and 5 mM Mn^{2+}/10 mM Mg^{2+} (◆) from the pH dependence of the reactivity of G_N relative to G in the reaction E·S·G_X → products: $k_{c,rel} = k_c^{G_N}/k_c^G$. Values of $k_c^{G_X}$ were determined with saturating E (50−200 nM) and G_X (2 mM) as described under Materials and Methods. The solid lines are the fit of the data to eq 5, derived from Scheme 1, and give observed pK_a values of E·S·G_N of 8.6, 7.1, and 4.9 at 2 mM Mg^{2+}, 100 mM Mg^{2+}, and 5 mM Mn^{2+}/10 mM Mg^{2+}, respectively (see Materials and Methods).

Placing the results of this section in the context of Figure 2 (thick arrows in foreground), $G_{NH_3^+}$ binds strongly to the E·S complex when metal site C is unoccupied, with a binding constant of $K_{b,o}^{G_{NH_3^+}} \geq 1000$ mM^{-1}. Mg^{2+} binds tightly to site C in E·S, with $K_{E\cdot S}^{Mg} \leq 2$ mM (see also ref *1*). Binding of Mg_C^{2+} weakens the affinity of $G_{NH_3^+}$, with $K_{b,Mg}^{G_{NH_3^+}} \leq 16$ mM^{-1}. A Mn^{2+} ion also binds strongly to site C, with a dissociation constant of $K_{E\cdot S}^{Mn} \leq 40$ μM for the E·S complex (*1*). Binding of $G_{NH_3^+}$ is weakened more than 100-fold upon binding of Mn_C^{2+}, with $K_{b,Mn}^{G_{NH_3^+}} \leq 7.6$ mM^{-1}. Conversely, the affinities of Mg^{2+} and Mn^{2+} for site C are weakened upon binding of $G_{NH_3^+}$, with $K_{E\cdot S\cdot G_{NH_3^+}}^{Mg} \geq 26$ mM^{-1} and $K_{E\cdot S\cdot G_{NH_3^+}}^{Mn} \geq$ 3.6 mM.

Effect of M_C on Deprotonation of $G_{NH_3^+}$. To ensure that the binding and reactivity of $G_{NH_3^+}$ or G_{NH_2} were followed in this and the preceding paper (*1*), it was crucial to determine the equilibrium for deprotonation of the 2′-NH_3^+ group of $G_{NH_3^+}$ and how M_C and the ribozyme active site perturb this equilibrium. The equilibrium constants for deprotonation of $G_{NH_3^+}$ in solution and in the E·S·G_N complexes were therefore determined with varying concentrations of metal ion.

(A) Deprotonation of $G_{NH_3^+}$ in Solution. The equilibrium constant for deprotonation of the 2′-amino group in solution has been determined above from the pH dependence of the binding of G_N, which gives $pK_a^{G_N} = 6.1$ (Figure 4). This value is similar to the pK_a of 6.2 for the 2′-amino group within a UpT dinucleotide determined by NMR spectroscopy (*45*). The solution pK_a of $G_{NH_3^+}$ is, of course, the same regardless of whether there is a metal ion bound at site C or whether this metal site is occupied by Mg^{2+} or Mn^{2+} (Figure 2, $pK_{a,o}^{G_N} = pK_{a,Mg}^{G_N} = pK_{a,Mn}^{G_N} = 6.1$).

(B) Deprotonation of E·S·$G_{NH_3^+}$ with Metal Site C Unoccupied, $pK_{a,o}^{E\cdot S\cdot G_N}$. As described above, the equilibrium constant for deprotonation of the -NH_3^+ group in the E·S·G_N complex can be determined from the pH dependence of the rate of the chemical step of G_N relative to G, $k_{c,rel}$ (Figure 3 above). The value of $pK_{a,o}^{E\cdot S\cdot G_N}$ was estimated from the pH dependence of $k_{c,rel}$ at the lowest Mg^{2+} concentration that ensures folding of the ribozyme [Figure 6, closed circles; 2 mM Mg^{2+} used herein (*46*, *47*)]. A fit of this pH dependence to the model of Scheme 1 gives an apparent pK_a value of 8.6 for the -NH_3^+ group at 2 mM Mg^{2+}. This value is a lower limit for $pK_{a,o}^{E\cdot S\cdot G_N}$, the p$K_a$ of the -NH_3^+ group in E·S·G_N with site C unoccupied, because Mg^{2+} is bound at site C in the E·S·G_{NH_2} complex under these conditions (Figure 2, $K_{E\cdot S\cdot G_{NH_2}}^{Mg} \leq 2$ mM; *1*).

(C) Deprotonation of E·S·$G_{NH_3^+}$ with Mg_C^{2+} Bound, $pK_{a,Mg}^{E\cdot S\cdot G_N}$. Analogously, the value of $pK_{a,Mg}^{E\cdot S\cdot G_N}$ was estimated from the pH dependence of $k_{c,rel}$ at 100 mM Mg^{2+} (Figure 6, open curves). The data were again analyzed according to the model of Scheme 1, giving an observed pK_a of 7.1 at 100 mM Mg^{2+}. This value is an upper limit for $pK_{a,Mg}^{E\cdot S\cdot G_N}$, the p$K_a$ of the -NH_3^+ group in E·S·G_N with Mg^{2+} bound at metal site C, because site C may not be saturated by Mg^{2+} in the E·S·$G_{NH_3^+}$ complex under these conditions (Figure 2, $K_{E\cdot S\cdot G_{NH_3^+}}^{Mg} \geq 26$ mM).

(D) Deprotonation of E·S·$G_{NH_3^+}$ with Mn_C^{2+} Bound, $pK_{a,Mn}^{E\cdot S\cdot G_N}$. This p$K_a$ value was estimated from the pH dependence of $k_{c,rel}$ in the presence of 5 mM Mn^{2+} (Figure 6, closed diamonds; 10 mM Mg^{2+} background). Analysis of the data according to the model of Scheme 1 gives an apparent pK_a value of 4.9. This value represents an upper limit for $pK_{a,Mn}^{E\cdot S\cdot G_N}$, the p$K_a$ of the -NH_3^+ group in E·S·G_N with Mn^{2+} bound at metal site C, as site C may not be saturated by Mn^{2+} in the E·S·$G_{NH_3^+}$ complex under these metal ion concentrations (Figure 2; $K_{E\cdot S\cdot G_{NH_3^+}}^{Mn} \geq 3.6$ mM).

The Oligonucleotide Substrate Accentuates the Competition between M_C and $G_{NH_3^+}$. In this section, we explore the effects of bound oligonucleotide substrate on the competition between M_C and $G_{NH_3^+}$ and identify the properties of S responsible for this effect. The oligonucleotide substrate binds the ribozyme in two steps (Figure 7; *48*−*52*). First, the open complex is formed [$(E\cdot S)_o$], in which S is held solely by base-pairing interactions with the internal guide sequence (IGS) of the ribozyme to form the P1 duplex. Second, the closed complex is formed [$(E\cdot S)_c$], in which the P1 duplex docks into the ribozyme core via tertiary interactions.

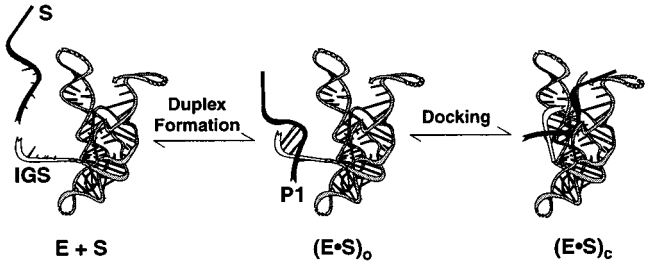

FIGURE 7: Two-step model for binding of oligonucleotide substrate. S (dark) first forms the open complex [$(E\cdot S)_o$] by base pairing with the internal guide sequence (IGS = GGAGGG; white) of E to form the P1 duplex. The P1 duplex then docks into the catalytic core via ternary interactions to form the closed complex [$(E\cdot S)_c$; *20*, *23*, *48*, *50*, and references cited therein].

[8] $K_{E\cdot S\cdot G_{NH_3^+}}^{Mn}$ is the Mn^{2+} dissociation constant from unoccupied metal site C, because Mg^{2+} is not bound at site C in the E·S·$G_{NH_3^+}$ complex at 10 mM Mg^{2+} (Figure 2, $K_{E\cdot S\cdot G_{NH_3^+}}^{Mg} \geq 26$ mM).

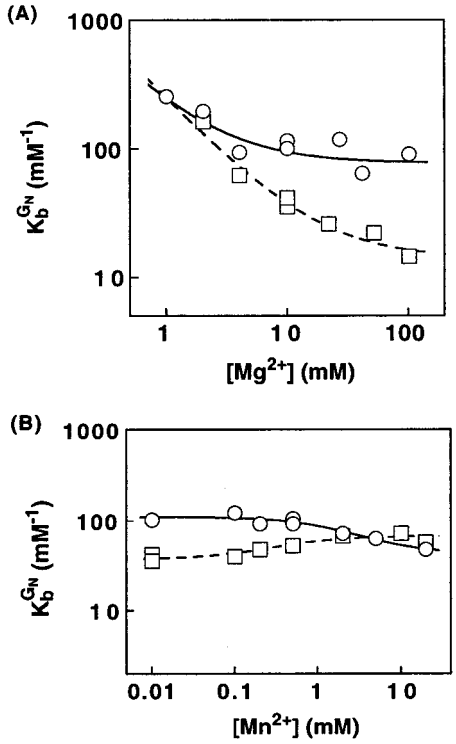

FIGURE 8: Effect of Mg^{2+} (A) and Mn^{2+} (B) on the equilibrium binding constant of $G_{NH_3^+}$ to the $(E{\cdot}S)_o$ complex (○) and the $(E{\cdot}P)_c$ complex (□), determined at pH 5.0 as described under Materials and Methods.[9] The Mn^{2+} concentration dependences in part B were determined in the presence of 10 mM Mg^{2+}. The lines are fits of the data to a model in which a single metal ion alters the binding of $G_{NH_3^+}$, analogous to Schemes 4 and 5.

(A) Effect of Mg^{2+} and Mn^{2+} on Binding of $G_{NH_3^+}$ to the $(E{\cdot}S)_o$ Complex. The results described in the previous sections were obtained with rSA_5 or -1d,rSA_5, oligonucleotide substrate that binds E in the closed complex, $(E{\cdot}S)_c$. To test whether docking of S influences the effect of M_C on $G_{NH_3^+}$ binding, the effect of metal ions on the binding of $G_{NH_3^+}$ to the $(E{\cdot}S)_o$ complex was determined (Figure 8).[9] The $(E{\cdot}S)_o$ complex was formed by using the oligonucleotide substrate -3m,rSA_5 (Chart 1). The 2′-OH at the -3 position is involved in tertiary stabilization of the closed complex; substitution of this 2′-OH with an $-OCH_3$ group disrupts docking of S, yielding a stable open complex (*23*, *52*, *53*, and references therein).

In contrast to the more than 60-fold weakened binding of $G_{NH_3^+}$ to the $(E{\cdot}S)_c$ complex upon binding of Mn^{2+} to site C (Figure 2, $K_{b,Mg}^{G_{NH_3^+}}$ vs $K_{b,o}^{G_{NH_3^+}}$), the binding of $G_{NH_3^+}$ to the $(E{\cdot}S)_o$ complex weakens less than 3-fold when [Mg^{2+}] is increased from 2 to 100 mM (Figure 8A, circles). Similarly, addition of up to 20 mM Mn^{2+} has only a 2-fold effect on the binding of $G_{NH_3^+}$ to $(E{\cdot}S)_o$ (Figure 8B, circles; 10 mM Mg^{2+}), in contrast to the more than 100-fold weakening of the binding of $G_{NH_3^+}$ to $(E{\cdot}S)_c$ upon binding of Mn_C^{2+} (Figure 2, $K_{b,Mn}^{G_{NH_3^+}}$ vs $K_{b,o}^{G_{NH_3^+}}$). Further, the binding of $G_{NH_3^+}$ weakens only above 2 mM Mn^{2+}, 10-fold above the dissociation constant for Mn_C^{2+} (*1*). Thus, the effect of Mn_C^{2+} on the binding of $G_{NH_3^+}$ may be even smaller than observed in Figure 8B.

The stronger binding of $G_{NH_3^+}$ to the ribozyme·substrate complex formed with -3m,rSA_5 (E·mS) than with rSA_5 (E·rS) at high concentrations of Mg^{2+} and Mn^{2+} suggests that docking of S is destabilized by bound $G_{NH_3^+}$. This may result in formation of the $E{\cdot}rS{\cdot}G_{NH_3^+}$ open complex, so that the observed effects of Mg^{2+} and Mn^{2+} on $G_{NH_3^+}$ binding to the E·rS complex described in the previous sections represent lower limits for the effect in the $(E{\cdot}S)_c$ complex. As noted above, the observed effects are also lower limits because of potential contributions from other metal ions and because Mn^{2+} induces deprotonation of bound G_N.

(B) Effect of Mg^{2+} and Mn^{2+} on the Binding of $G_{NH_3^+}$ to the E·P Complex. The larger effects of Mg^{2+} and Mn^{2+} on the binding of $G_{NH_3^+}$ to the $(E{\cdot}S)_c$ than the $(E{\cdot}S)_o$ complex could arise from docking of the P1 duplex at the ribozyme core or from more localized interactions with the reactive portion of S. To differentiate between these possibilities, we measured the effect of metal ions on the binding of $G_{NH_3^+}$ to the ribozyme·oligonucleotide product (E·P) complex. In E·P, the P1 duplex is stably docked at the active site (*22*, *23*), but the reactive phosphoryl group and the 3′-terminal A residues are removed and replaced by a hydroxyl group (Chart 1). The closed complex formed with rP, $(E{\cdot}P)_c$, is 40-fold more stable than that formed with rSA_5; thus, the $(E{\cdot}P)_c$ complex is favored by $\sim 10^2$-fold relative to the $(E{\cdot}P)_o$ complex (10 mM Mg^{2+}; *22* and unpublished results). This suggests that the modest effects of Mg^{2+} and Mn^{2+} on $G_{NH_3^+}$ binding to the E·P complex would not be sufficient to disrupt docking of rP; thus, the observed effects represent effects within the $(E{\cdot}P{\cdot}G_{NH_3^+})_c$ complex (Figure 8, ≤10-fold effects).

The affinity of $G_{NH_3^+}$ for $(E{\cdot}P)_c$ weakens ~10-fold when [Mg^{2+}] is increased from 2 to 100 mM (Figure 8A, squares), 6-fold less than the effect of Mg^{2+} on the binding of $G_{NH_3^+}$ to $(E{\cdot}S)_c$ (Figure 2, $K_{b,Mg}^{G_{NH_3^+}}$ vs $K_{b,o}^{G_{NH_3^+}}$). The effect of Mg^{2+} on the binding of $G_{NH_3^+}$ to $(E{\cdot}P)_c$ could arise from the Mg^{2+} bound at site C or from other Mg^{2+} ion(s) within the $E{\cdot}P{\cdot}G_{NH_3^+}$ complex. Surprisingly, addition of Mn^{2+}, which binds 50-fold stronger than Mg^{2+} to metal site C in the $(E{\cdot}P)_c$ complex, does not weaken the binding of $G_{NH_3^+}$ to $(E{\cdot}P)_c$ even at concentrations as high as 20 mM [Figure 8B, squares; 10 mM Mg^{2+}; $K_{E{\cdot}P}^{Mn,app} = 0.19$ mM (*1*)]. In contrast, Mn_C^{2+} weakens binding of $G_{NH_3^+}$ to the $(E{\cdot}S)_c$ complex more than 100-fold (Figure 2, $K_{b,Mn}^{G_{NH_3^+}}$ vs $K_{b,o}^{G_{NH_3^+}}$). The substantially smaller effect of Mn^{2+} on the binding of $G_{NH_3^+}$ to $(E{\cdot}P)_c$ than to $(E{\cdot}S)_c$ suggests that the negatively charged reactive phosphoryl group of S increases the antagonistic effects between $G_{NH_3^+}$ and Mn^{2+} bound at site C, instead of ameliorating their apparent repulsion.

[9] The binding of G_N to $(E{\cdot}S)_o$ at low pH is stronger than at high pH over the entire range of Mg^{2+} and Mn^{2+} concentrations investigated [$K_b^{G_N} \geq 60$ mM^{-1} at pH 4.7−5.0 (Figure 8); $K_b^{G_N} \leq 9.1$ mM^{-1} above pH 7.9 (*1* and unpublished results)]; this suggests that $G_{NH_3^+}$ binds more strongly to the $(E{\cdot}S)_o$ complex than G_{NH_2}. The binding of G_N to $(E{\cdot}S)_o$ observed below pH 5.0 can therefore be attributed to $G_{NH_3^+}$, with negligible contribution from the small fraction of G_{NH_2} that is present (≤ 0.04; $pK_a^{G_N} = 6.1$). Similarly, the binding of G_N to E·P observed at low pH (5.0) can be attributed to $G_{NH_3^+}$ because $G_{NH_3^+}$ binds more strongly to E·P than G_{NH_2} over the range of Mg^{2+} and Mn^{2+} concentrations investigated [$K_b^{G_N} \geq 16$ mM^{-1} at pH 5.0 (Figure 8); $K_b^{G_N} \approx 3.4$ mM^{-1} above pH 7.9 (*1* and unpublished results)].

Scheme 6

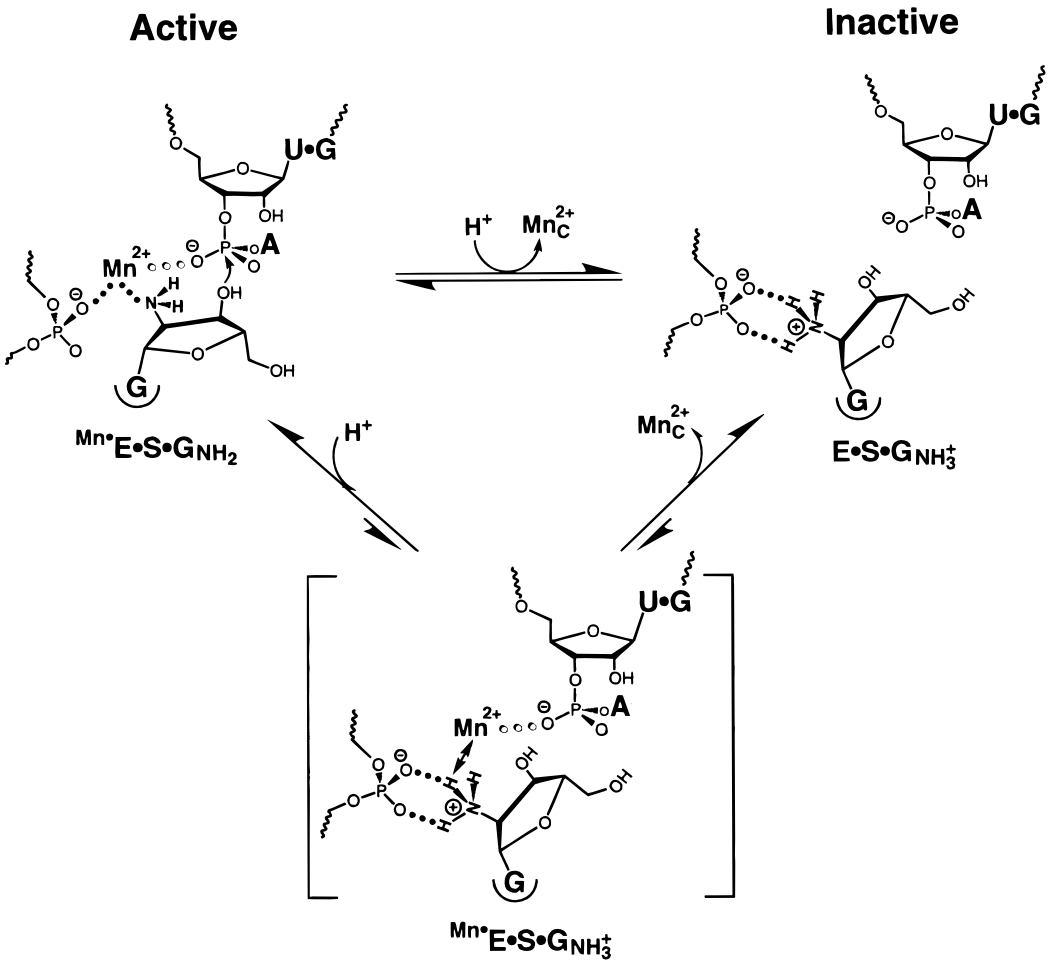

DISCUSSION

The abillity of a protonated amine to probe the local electrostatic environment within a structured RNA was explored in this work using $G_{NH_3^+}$, an analogue of the guanosine nucleophile in the *Tetrahymena* ribozyme reaction. Catalysis provides a sensitive readout for the electrostatic interactions within the active site, and the well-characterized *Tetrahymena* ribozyme has further allowed quantitation of these effects in individual complexes, thereby revealing factors that influence the electrostatic interactions of $G_{NH_3^+}$. The results of this investigation provide information about the electrostatic environment within the *Tetrahymena* ribozyme active site and allow further characterization of the metal ion, M_C, that interacts with the 2′-moiety of guanosine. These experiments also provide critical controls necessary for establishing conditions for study of G_{NH_2} in the preceding paper (*1*).

The results herein show that $G_{NH_3^+}$ binds to the $(E{\cdot}S)_c$ complex more than 200-fold stronger than G or G_{NH_2}, with $K_d^{G_{NH_3^+}} \leq 1$ μM at low concentrations of metal ion. This remarkably tight binding suggests that the positively charged 2′-NH_3^+ group of $G_{NH_3^+}$ interacts with one or more negatively charged phosphoryl groups near the 2′-moiety of G. In the $(E{\cdot}P)_c$ complex, in which the reactive phosphoryl group is removed, the binding of $G_{NH_3^+}$ remains more than 50-fold stronger than G and G_{NH_2}, with a dissociation constant of ≤ 6 μM at low metal ion concentrations. The strong binding of $G_{NH_3^+}$ to E·P suggests that $G_{NH_3^+}$ interacts with at least one active site phosphoryl group distinct from the reactive phosphoryl group of S. This interaction is depicted by the closed dots between $G_{NH_3^+}$ and a nearby phosphoryl group in the model of Scheme 6 ($E{\cdot}S{\cdot}G_{NH_3^+}$).

Binding of $G_{NH_3^+}$ is weakened more than 10^2-fold upon addition of Mg^{2+} and Mn^{2+}, strongly suggesting that the metal ions bound at site C and $G_{NH_3^+}$ compete with one another for binding. In contrast, Mn^{2+} at site C increases the affinity of G_{NH_2} (*1*). These observations, summarized in Figure 2, are accounted for by the model of Scheme 6. As shown in the preceding paper, Mn_C^{2+} interacts with the 2′-NH_2 group of G_{NH_2} in the active complex (^{Mn}•E·S·G_{NH_2}). Protonation of the 2′-amino group to give $G_{NH_3^+}$ prevents this favorable interaction; further, this creates electrostatic repulsion between the positively charged -NH_3^+ group and Mn_C^{2+}, depicted by '↔' in the ^{Mn}•E·S·$G_{NH_3^+}$ complex. Thus, this species does not accumulate: either the proton is lost to give $^{Mn\cdot}$E·S·G_{NH_2} or the metal is displaced to give $E{\cdot}S{\cdot}G_{NH_3^+}$, depending on the pH and Mn^{2+} concentration. In addition, $G_{NH_3^+}$ may compete for one or more phosphoryl groups that normally provide ligands for metal ion C in the active complex. Such phosphoryl ligands could also contribute to the strong binding of Mn^{2+} to site C (*1*).

Phylogenetic and low-resolution X-ray models suggest the presence of several phosphoryl groups in the active site region, those of residues A306, A261, A207, and C208 (*54*,

55). In addition, thio substitution at these phosphoryl groups is deleterious to intron function and can be rescued by addition of Mn^{2+} (*5*, *56*, *57*), consistent with ligation of active site metal ions by these phosphoryl groups.

The $E{\cdot}S{\cdot}G_{NH_3^+}$ complex is at least 10^4-fold less reactive than the corresponding complex with G or G_{NH_2}, and this species is therefore labeled 'Inactive' in Scheme 6. The low reactivity of $G_{NH_3^+}$ provides additional support for a crucial role of M_C in catalysis by the *Tetrahymena* ribozyme (*1*, *35*). M_C could coordinate to the 3′-OH of G, along with metal ion B, to help deprotonate and activate the 3′-OH for nucleophilic attack (Figure 1; *1*, *35*). Alternatively or in addition, loss of M_C and interaction of the $-NH_3^+$ group with active site phosphoryl groups could misalign the 3′-OH of $G_{NH_3^+}$, thereby preventing efficient reaction (Scheme 6; *1*).

Previous results have indicated that there is coupled binding between the guanosine nucleophile and the oligonucleotide substrate, and that this coupling involves the reactive phosphoryl group, the 2′-moiety of G, and M_C (*1*, *38*, *49*). These observations suggested the presence of a network of interactions within the active site. The results with $G_{NH_3^+}$ provide additional evidence for such a network, as described below.

Binding of $G_{NH_3^+}$ to the $(E{\cdot}S)_c$ complex is weakened more than 10^2-fold by Mg_C^{2+} and Mn_C^{2+} (Figure 2, $K_{b,o}^{G_{NH_3^+}}$ vs $K_{b,Mg}^{G_{NH_3^+}}$ and $K_{b,Mn}^{G_{NH_3^+}}$); this corresponds to unfavorable interaction free energies of at least 2.5 and 3.2 kcal/mol of $G_{NH_3^+}$ with Mg_C^{2+} and Mn_C^{2+}, respectively. In contrast, M_C weakens the binding of $G_{NH_3^+}$ to a much smaller extent, less than 5-fold, with the $(E{\cdot}P)_c$ complex which lacks the reactive phosphoryl group. Thus, the presence of the reactive phosphoryl group substantially accentuates the electrostatic repulsion between $G_{NH_3^+}$ and M_C. This suggests that interactions involving the reactive phosphoryl group are responsible for positioning within the active site, as previously suggested (*1*). Strong electrostatic repulsion is expected when groups are positioned close to one another and when there is a substantial energetic penalty for rearrangement to avoid such repulsion (*26*−*29*). Thus, the results with $G_{NH_3^+}$ as an electrostatic probe suggest that there is substantial active site rigidity within the *Tetrahymena* ribozyme. This rigidity may reflect the ability of this RNA enzyme to use a network of interactions to position substrates with respect to one another and with respect to catalytic groups (*22*).

ACKNOWLEDGMENT

We are grateful to J. Piccirilli for helpful discussions, F. Eckstein for the gift of 2′-aminoguanosine, L. Beigelman for oligonucleotide substrates, and members of the Herschlag lab for comments on the manuscript.

REFERENCES

1. Shan, S., and Herschlag, D. (1999) *Biochemistry 38*, 10958−10975.
2. Beebe, J. A., Kurz, J. C., and Fierke, C. A. (1996) *Biochemistry 35*, 10493−10505.
3. Cate, J. H., and Doudna, J. A. (1996) *Structure 4*, 1221−1229.
4. Cate, J. H., Gooding, A. R., Podell, E., Zhou, K., Golden, B. L., Kundrot, C. E., Cech, T. R., and Doudna, J. A. (1996) *Science 273*, 1678−1685.
5. Christian, E. L., and Yarus, M. (1993) *Biochemistry 32*, 4475−4480.
6. Correll, C. C., Freeborn, B., Moore, P. B., and Steitz, T. A. (1997) *Cell 91*, 705−712.
7. Draper, D. E. (1996) *Trends Biochem. Sci. 21*, 145−149.
8. Fourmy, D., Recht, M. I., Blanchard, S. C., and Puglisi, J. D. (1996) *Science 274*, 1367−1371.
9. Fourmy, D., Recht, M., and Puglisi, J. D. (1998) *J. Mol. Biol. 276*, 347−362.
10. Hermann, T., and Westhof, E. (1998) *J. Mol. Biol. 276*, 903−912.
11. Pley, H. W., Flaherty, K. M., and McKay, D. B. (1994) *Nature 372*, 68−74.
12. Pan. T., Long, D. M., and Uhlenbeck, O. C. (1993) in *The RNA World*, pp 271−302, Cold Spring Harbor Laboratory Press, Cold Spring Harbor, NY.
13. Quigley, G. J., Teeter, M. M., and Rich, A. (1978) *Proc. Natl. Acad. Sci. U.S.A. 75*, 64−68.
14. Saenger, W. (1984) in *Principles of Nucleic Acid Structure*, pp 201−219, Springer-Verlag, New York.
15. Yamada, A., Akasaka, K., and Hatano, H. (1976) *Biopolymers 15*, 1315−1331.
16. Cech, T. R., and Golden, B. L. (1999) in *The RNA World*, pp 321−349, Cold Spring Harbor Laboratory Press, Cold Spring Harbor, NY.
17. Kieft, J. S., and Tinoco, I., Jr. (1997) *Structure 5*, 713−721.
18. Allain, F. H.-T., and Varani, G. (1995) *Nucleic Acids Res. 23*, 341−350.
19. Patel, D. J., Suri, A. K., Jiang, F., Jiang, L., Fan, P., Kumar, R. A., and Nonin, S. (1997) *J. Mol. Biol. 272*, 645−664.
20. Szewczak, A. A., Ortoleva-Donnelly, L., Ryder, S. P., Moncoeur, E., and Strobel, S. A. (1998) *Nat. Struct. Biol. 5*, 1037−1042.
21. Zimmermann, G. R., Jenison, R. D., Wick, C. L., Simorre, J.-P., and Pardi, A. (1997) *Nat. Struct. Biol. 4*, 644−649.
22. Narlikar, G. J., Gopalakrishnan, V., McConnel, T. S., Usman, N., and Herschlag, D. (1995) *Proc. Natl. Acad. Sci. U.S.A. 92*, 3668−3672.
23. Narlikar, G. J., Khosla, M., Usman, N., and Herschlag, D. (1997) *Biochemistry 36*, 2465−2477.
24. Narlikar, G. J., and Herschlag, D. (1997) *Annu. Rev. Biochem. 66*, 19−59.
25. Narlikar, G. J., and Herschlag, D. (1998) *Biochemistry 37*, 9902−9911.
26. Gilson, M. K., and Honig, B. H. (1987) *Nature 330*, 84−88.
27. Honig, B., and Nicholls, A. (1995) *Science 268*, 1144−1149.
28. King, G., Lee, F. S., and Warshel, A. (1991) *J. Chem. Phys. 95*, 4366−4377.
29. Warshel, A., and Russell, S. T. (1984) *Q. Rev. Biophys. 17*, 283−422.
30. Herschlag, D., and Cech, T. R. (1990) *Biochemistry 29*, 10159−10171.
31. Herschlag, D., and Cech, T. R. (1990) *Biochemistry 29*, 10172−10180.
32. Cech, T. R., and Herschlag, D. (1996) in *Nucleic Acids and Molecular Biology*, pp 1−17, Springer, Berlin.
33. Bass, B. L., and Cech, T. R. (1986) *Biochemistry 25*, 4473−4477.
34. Tanner, N. K., and Cech, T. R. (1987) *Biochemistry 26*, 3330−3340.
35. Sjögren, A.-S., Pettersson, E., Sjöberg, B.-M., and Strömberg, R. (1997) *Nucleic Acids Res. 25*, 648−653.
36. Zaug, A. J., Grosshans, C. A., and Cech, T. R. (1988) *Biochemistry 27*, 8924−8931.
37. Herschlag, D., Eckstein, F., and Cech, T. R. (1993) *Biochemistry 32*, 8312−8321.
38. McConnell, T. S., Cech, T. R., and Herschlag, D. H. (1993) *Proc. Natl. Acad. Sci. U.S.A. 90*, 8362−8366.
39. Knitt, D. S., and Herschlag, D. (1996) *Biochemistry 35*, 1560−1570.
40. Herschlag, D., and Khosla, M. (1994) *Biochemistry 33*, 5291−5297.
41. Herschlag, D., Eckstein, F., and Cech, T. R. (1993) *Biochemistry 32*, 8299−8311.
42. Herschlag, D., Piccirilli, J. A., and Cech, T. R. (1991) *Biochemistry 30*, 4844−4854.

43. McConnell, T. S. (1995) Ph.D. Thesis, University of Colorado, Boulder, CO.
44. Fersht, A. (1984) in *Enzyme Structure and Mechanism*, p 161, W. H. Freeman and Company, New York.
45. Aurup, H., Tuschl, T., Benseler, F., Ludwig, J., and Eckstein, F. (1994) *Nucleic Acids Res. 22*, 20−24.
46. Celander, D. W., and Cech, T. R. (1991) *Science 251*, 401−407.
47. Wang, J. F., and Cech, T. R. (1994) *J. Am. Chem. Soc. 116*, 4178−4182.
48. Bevilacqua, P. C., Kierzek, R., Johnson, K. A., and Turner, D. H. (1992) *Science 258*, 1355−1358.
49. Bevilacqua, P. C., Li, Y., and Turner, D. H. (1994) *Biochemistry 33*, 11340−11348.
50. Herschlag, D. (1992) *Biochemistry 31*, 1386−1398.
51. Li, Y., Bevilacqua, P. C., Mathews, D., and Turner, D. H. (1995) *Biochemistry 34*, 14394−14399.
52. Narlikar, G. J., and Herschlag, D. (1996) *Nat. Struct. Biol. 3*, 701−710.
53. Knitt, D. S., Narlikar, G. J., and Herschlag, D. (1994) *Biochemistry 33*, 13864−13879.
54. Michel, F., and Westhof, E. (1990) *J. Mol. Biol. 216*, 585−610.
55. Golden, B. L., Gooding, A. R., Podell, E. R., and Cech, T. R. (1998) *Science 282*, 259−264.
56. Waring, R. B. (1989) *Nucleic Acids Res. 17*, 10281−10294.
57. Christian, E. L., and Yarus, M. (1992) *J. Mol. Biol. 228*, 743−758.
58. Strobel, S. A., and Cech, T. R. (1995) *Science 267*, 657−679.
59. Strobel, S. A., and Cech, T. R. (1996) *Biochemistry 35*, 1201−1211.
60. Strobel, S. A., and Ortoleva-Donnelly, L. (1999) *Chem. Biol. 6*, 153−165.
61. Piccirilli, J. A., Vyle, J. S., Caruthers, M. H., and Cech, T. R. (1993) *Nature 361*, 85−88.
62. Weinstein, L. B., Jones, B. C., Cosstick, R., and Cech, T. R. (1997) *Nature 388*, 805−808.

BI9903897